Supplementary information for the paper entitled: Electric fields that "arrive" before the time-derivative of the Magnetic field prior to major earthquakes

P. A. Varotsos,[1,*] N. V. Sarlis,[1] and E. S. Skordas[1]

[1] *Solid State Section, Physics Department, University of Athens, Panepistimiopolis, Zografos 157 84, Athens, Greece*

The present supplementary material is organized as follows: the sites of the electrodes as well as a few points on the instrumentation are presented in Section I. Section II clarifies how the cross-correlation values have been calculated in the main text. Examples of recordings from nearby artificial noises and magnetotelluric (MT) variations (i.e., induced by variations of the earth's magnetic field) are presented in Section III. Further details on the recordings (and their analysis) of the electric and magnetic field variations, that have been found to precede the EQ of magnitude M≈6.6 discussed in the main text, are described in Sections IV and V. Finally, in Section VI, we give details on the procedure for the calculation of the electromagnetic fields, in the time-domain, for the model discussed in the main text. Furthermore, in the same Section, recent field measurements, which lend support to the latter model, are forwarded.

I. THE INSTRUMENTATION.

The electric field measurements have been carried out by means of short and long dipoles; the sites of their electrodes are shown in Fig.1. The magnetometers are located in the middle of the short dipoles' array (i.e., close to the middle of $N'S'$-see Fig.1(a)- which lies between the sites 'b' and 'c').

During the collection of the SES activities discussed in the main text, the permanent recording of the magnetic field variations at Ioannina station (IOA) was solely carried out by three DANSK coil magnetometers (DMM). Furthermore, since 1996 the MT-1 system of Electro-Magnetic Instruments (EMI) has been also used. Concerning the calibration of DMM (details are given in Ref. 7 of the main text), beyond a laboratory calibration, an in situ (i.e., at IOA) calibration was performed by comparing the DMM recordings $V_m(t)$ to those of EMI-magnetometers (hereafter called EMM) and relying on the accurate laboratory calibration of the latter (which has been reported by the manufacturer[1]). This calibration led to a Heaviside (or unit step) response function $H(t)$:

$$V_m(t) = \int_{-\infty}^{\infty} H(\xi)\frac{dB}{dt}(t-\xi)d\xi, \qquad (1)$$

that vanishes for $t < 0$, while for $t \geq 0$

$$\begin{aligned} H(t) &= A\frac{\tau_d^4}{(\tau_d-\tau_r)^4}\left[\exp\left(-\frac{t}{\tau_d}\right) - \exp\left(-\frac{t}{\tau_r}\right)\right] \\ &- A\frac{\tau_d^3}{(\tau_d-\tau_r)^3}\frac{t}{\tau_r}\exp\left(-\frac{t}{\tau_r}\right) \\ &- \frac{A}{2}\frac{\tau_d^2}{(\tau_d-\tau_r)^2}\left(\frac{t}{\tau_r}\right)^2\exp\left(-\frac{t}{\tau_r}\right) \\ &- \frac{A}{6}\frac{\tau_d}{(\tau_d-\tau_r)}\left(\frac{t}{\tau_r}\right)^3\exp\left(-\frac{t}{\tau_r}\right) \qquad (2) \end{aligned}$$

with $\tau_d \approx 0.025$s and $\tau_r \approx 0.007$s (see Ref. 7 of the main text). In summary, this calibration showed that DMM magnetometers act as dB/dt detectors for periods larger than around half a second; furthermore their output is "neutralized" 200ms after the "arrival" of a Heaviside unit step magnetic variation, i.e, $B(t) = B_0\Theta(t)$, where $\Theta(t)$ is the Heaviside (or unit step) function. This property is of central importance towards studying the time-difference Δt between the "arrival" times of the variations of the electric and those of the magnetic field.

II. CLARIFICATIONS ON THE CALCULATION OF THE CROSS-CORRELATION

We note that a key quantity for the study of the time-difference Δt between two time-series $x_i, y_i, i = 1, 2, \ldots N$ is the cross-correlation function "cr"[$\equiv X_c(x, y; \Delta t)$]. This is defined through the cross-covariance function

$$\begin{aligned} c_{xy}(k) &= \frac{\sum_{t=1}^{N-k}(x_t - \langle x\rangle)(y_{t+k} - \langle y\rangle)}{N}, k = 0, 1, .., N \\ &= \frac{\sum_{t=1-k}^{N}(x_t - \langle x\rangle)(y_{t+k} - \langle y\rangle)}{N}, k = -1, .., 1-N \end{aligned}$$

scaled by the variances of the two series:

$$X_c(x, y; \Delta t) = \frac{c_{xy}(\Delta t)}{\sqrt{c_{xx}(0)c_{yy}(0)}}, \qquad (3)$$

where $\langle x\rangle$ and $\langle y\rangle$ stand for the time-averages of x_i and y_i, respectively.

It might be possible that the two time-series are autocorrelated and the direct cross-correlation function between them might give a misleading indication of their interrelation (examples can be found in Refs. 7,10 of the main text and in Fig. 4 that will be discussed later). One solution to this problem is "prewhitening". In this procedure, in order to transform the first time-series to a non-autocorrelated one, an n-th order autoregressive [AR(n)] model is applied. This reduces the residuals to white noise with no autocorrelation at all non-zero time

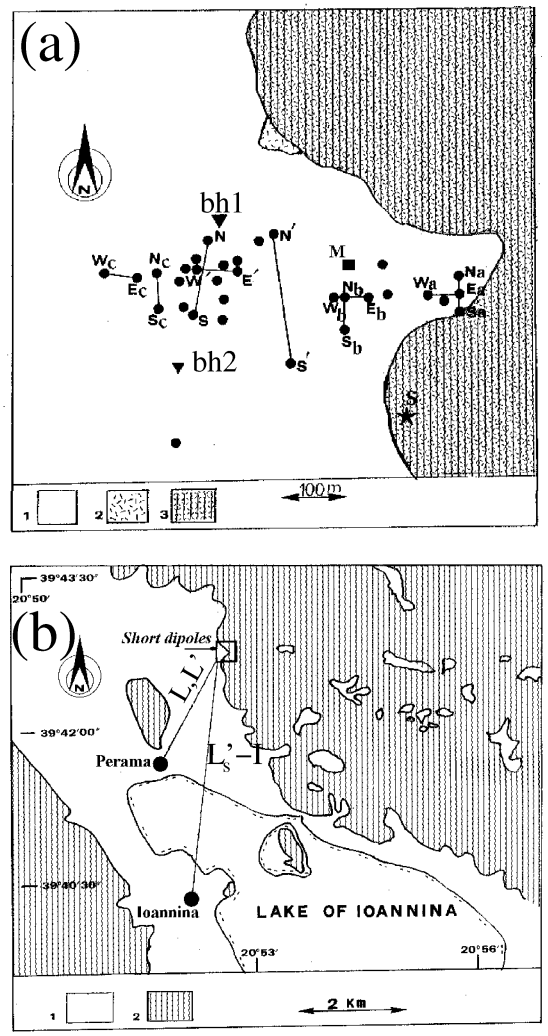

FIG. 1: Configuration of short (a) and long (b) dipoles at IOA (map modified from Ref.2 of the main text). In (a), the two solid inverted triangles stand for the two boreholes bh1, bh2 (of depth h=50 m) and the square (M) for the site of the hut. In (a), the short dipoles with subscripts b, c are those located at the sites 'b' and 'c', respectively. Concerning the geology: (a): (1) alluvial deposits, (2) flysch of the Ioanian unit, (3) limestones; (b): (1) quaternary sedimentary deposits, (2) alpine formation of the Ioanian unit (mainly limestones).

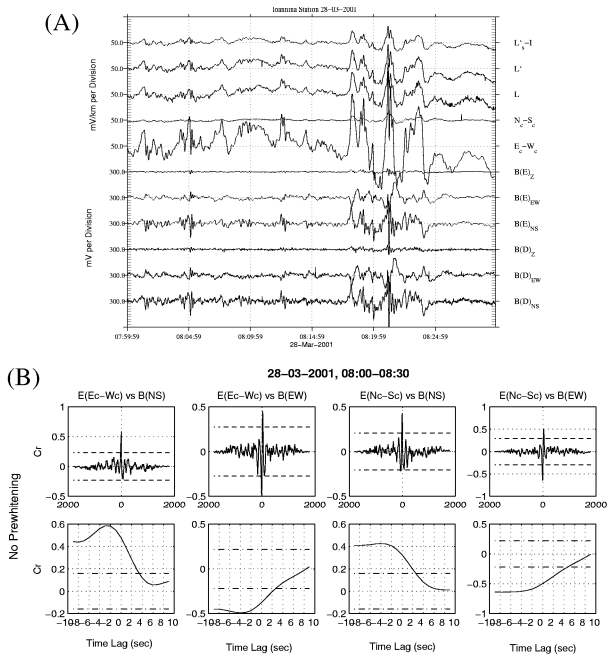

FIG. 2: (A) An example of MT disturbance recorded at IOA on March 28, 2001, with the permanently operating Campbell Scientific Datalogger 21X acquisition system (1 sample/sec) by using both types of coil magnetometers (i.e., the lower three channels correspond to DMM, while the next three to EMM). (B) Calculated values of "cr" between one horizontal E-field component and one B-field component versus their time-difference Δt (upper: Δt from -2000 to 2000 sec; below: Δt from -10 to 10 sec). Only the DMM recordings have been used in the calculation. Broken horizontal lines correspond to the 99% confidence level.

lags $\Delta t \neq 0$. Then, the second time-series is also filtered with the same model and cross correlation is found between the two filtered time-series.

III. THE TIME-DIFFERENCE BETWEEN THE TWO FIELDS DUE TO NEARBY ARTIFICIAL SOURCES OR MT VARIATIONS

Concerning the usual nearby (i.e., due to sources lying at distances $\lesssim$ 10km from the measuring site) artificial noises, the electric variations "arrive simultaneously" (i.e., with a time-difference appreciably smaller than 1 sec) with the magnetic ones detected by either DMM or EMM. As to the MT disturbances, for periods larger than 1 sec, the DMM recordings lead the electric ones by a measurable time-difference. These have been both assured (see Ref. 7 of the main text) by calculating the cross-correlation coefficient ("cr") between the time-series of one of the two horizontal components of the electric field and one of the three magnetic components.

As an example, Fig. 2A shows an MT disturbance simultaneously recorded on both types of coil magnetometers, i.e., DMM and EMM. The recordings of 11 (out of 16) channels are depicted as follows: the lower 3 channels correspond to the three DMM labeled here $B(D)_{NS}$, $B(D)_{EW}$ and $B(D)_Z$ respectively, and the next 3 channels to those of EMM (labeled with E in a parenthesis); the 7th and 8th channel (from the bottom) correspond to two short electric dipoles of length 50m [deployed along EW and NS directions at the site 'c' of IOA, see Fig.1(a)], while the upper 3 channels correspond to the three long dipoles (L, L′ and L'_s-I) with lengths $\approx$ 2, 2 and 5 km respectively, see Fig. 1(b). Figure 2B shows the calculated "cr" values between the time-series of the electric field variations and the DMM recordings versus Δt. An

inspection of this figure reveals that the magnetic field recordings "precede" markedly those of the electric field; this can be understood by recalling that, for the periods of the order of several seconds visualized in Fig. 2A, the DMM act as dB/dt detectors (as mentioned in Section I).

IV. THE VARIATIONS OF THE ELECTRIC AND MAGNETIC FIELD OBSERVED DUE TO SES ACTIVITIES

The 6.6 EQ that occurred on May 13,1995, was preceded, as mentioned in the main text, by two strong SES activities recorded at IOA station (see Ref. 2 of the main text) on April 18 and 19, 1995. The latter activity is shown in Fig. 1 of the main text, while here Fig. 3 depicts the SES activity on April 18, 1995. The following seven (out of 16) channels are depicted: the two horizontal DMM, labeled here B_{EW} and B_{NS}, (unfortunately, the vertical DMM was not properly operating during this time period), two short electric dipoles at site 'c' (labeled E_c-W_c and N_c-S_c, see Fig.1(a)) and the three long electric dipoles L, L′ and L'_s-I mentioned above (see Fig.1(b)).

Figure 4 depicts, for the SES activity on April 18, 1995, the "cr"-values, calculated [either with no prewhitening or after prewhitening, using the `cra` function of MATLAB of the MATHWORKS Inc. with an AR(10) model] between the following two time-series versus Δt: one component of the electric field (at site 'c') and one component of the horizontal DMM. An inspection of these results, reveals that the electric field variations precede the magnetic ones by a Δt of around one to two seconds,

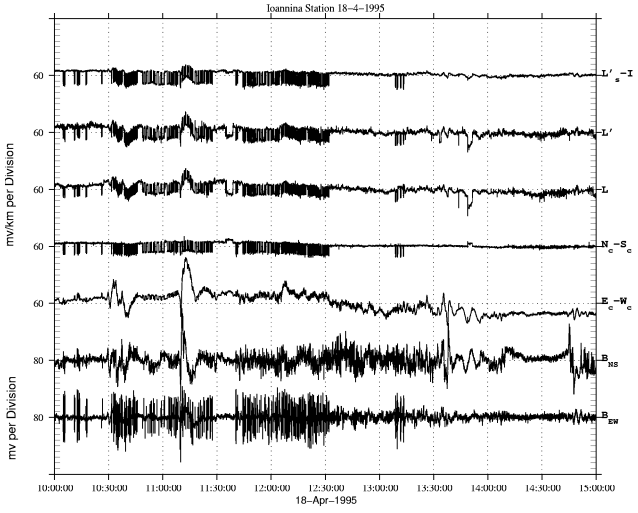

FIG. 3: The SES activity recorded (with 1 sample/sec) at IOA on April 18, 1995. The scale of 80mV in the lower two channels corresponds to dB/dt=0.4nT/sec, for a constantly increasing magnetic variation (see Refs 11, 13 of the main text).

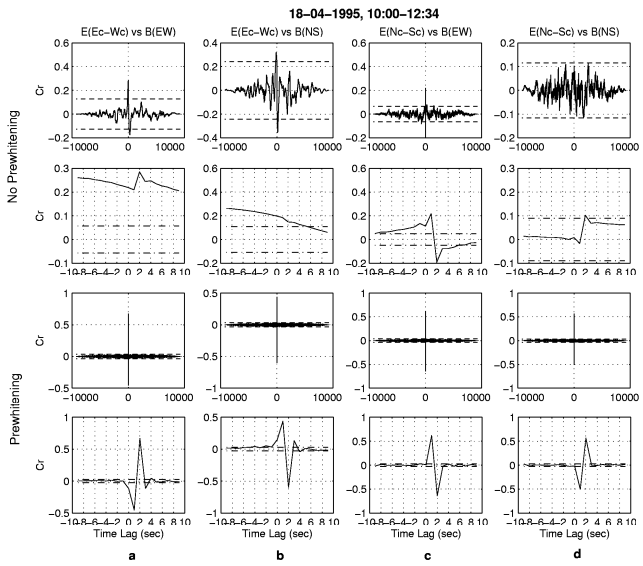

FIG. 4: The calculated "cr" values between one E-field component (at site 'c') and one B-field component (recorded by DMM) versus their time-difference Δt for the SES activity recorded at IOA on April 18, 1995. Upper (first) row: values calculated without prewhitening for Δt between -10000 and 10000 sec second row: the "cr" values calculated as in the first row, but now depicted in an expanded time scale, i.e., between -10 and 10 sec; third and fourth row: they depict the results of the upper two rows after prewhitening. Broken horizontal lines correspond to the 99% confidence level.

thus agreeing with the results obtained for the SES activity of April 19, 1995, described in the main text. We emphasize that the same Δt-values are obtained when studying the "cr" values of portions of the SES activities on April 18 or April 19, see Figs. 5A and 5B, respectively.

As discussed in the main text, in order to study whether the observed time-difference Δt was due to the "initiation" or "cessation" of the pulses, the "derivative" time-series of the central differences DtE [$\mathrm{DtE}_i \equiv (E_{i+1} - E_{i-1})$] were constructed from the electric field data. From DtE, the time-series of positive Dt-values, $\mathrm{DtE}_i\Theta(\mathrm{DtE}_i)$, and negative Dt-values, $\mathrm{DtE}_i\Theta(-\mathrm{DtE}_i)$, can be constructed. The series of positive (negative) Dt-values as mentioned in the main text marks the cessation (initiation) of the pulses of the SES activity. Figure 6, depicts for the SES activity on April 18, 1995, the "cr"-values calculated (without prewhitening) between the time-series of the derivative (Dt) of each one of the components of the E-field and each one of the recordings of the two horizontal DMM. The same Δt-values are obtained considering the time-series of either positive Dt-values or negative Dt-values (see the upper two rows or the lower two ones, respectively, in Fig. 6). These results agree with the relevant results for the SES activity on April 19, 1995, that have been presented in Fig.2(b) of the main text.

In order to exclude the possibility that the above Δt-

values could have arisen from the measuring system the response of the latter to the MT variations, that have been recorded during the *same* period (i.e., just before and after the SES activities), was investigated, as mentioned in the main text. For example, we consider an MT change, with a duration of around 10 min, just before the initiation of the SES activity on April 19, 1995. This MT variation is shown, in an expanded time scale, in Fig. 7A. The corresponding "cr" values between each component of the E-field and each component of the B-field are depicted in Fig. 7B and show that the DMM recordings lead the electric ones, as mentioned in Section III and also explained in the main text.

V. THE TIME DIFFERENCE Δt IS NOT SIGNIFICANTLY AFFECTED BY THE ORIENTATION (AND THE LENGTH) OF THE MEASURING ELECTRIC DIPOLES

Figure 3 of the main text shows a 50 seconds excerpt of the SES activity of April 19. Beyond the five electric dipoles (E_c-W_c, N_c-S_c, L, L' and L's-I) mentioned in Fig.1 of the main text, recordings of the following five additional short electric dipoles were shown [see also

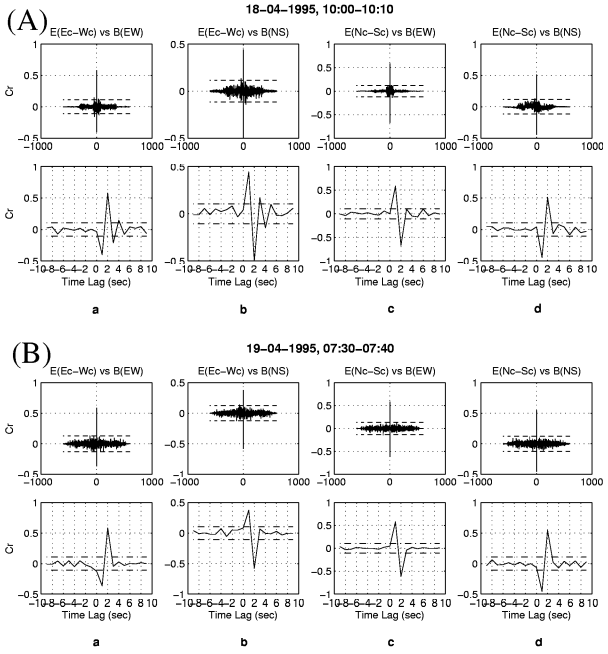

FIG. 5: The calculated "cr"-values (after prewhitening) between one E-field component and one B- field component (recorded by DMM) versus their time-difference Δt. The calculation was made only for a 10 min portion (600 data points) of the SES activities recorded on April 18 (A) and April 19, 1995 (B), respectively. In both cases, (A) , (B), the first row shows the results for Δt between -1000 and 1000 sec, while the second row depicts the range of Δt between -10 and 10 sec. Broken horizontal lines correspond to the 99% confidence level.

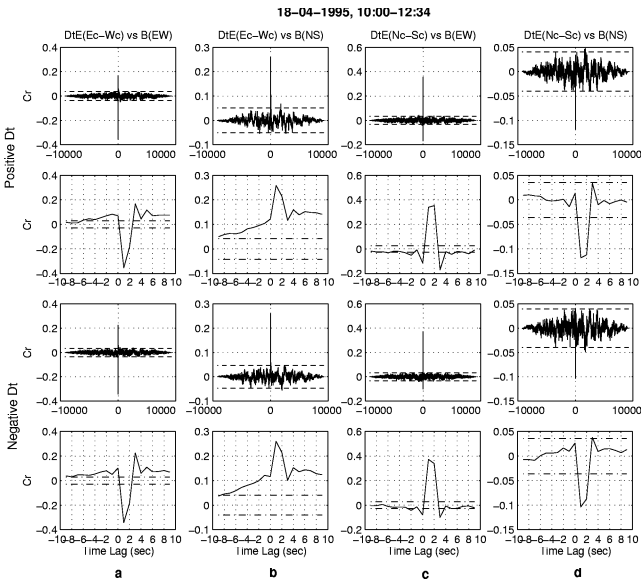

FIG. 6: The calculated "cr" between the following two time-series: (i)the derivative (Dt) of one E-field component and (ii)one B-field component (recorded by DMM), versus their time-difference Δt for the SES activity of April 18. Upper (first) row: values calculated for positive Dt without prewhitening and for Δt between -10000 sec and 10000 sec; second row: the "cr" values calculated as in the first row, but now depicted in an expanded time scale, i.e., between -10 and 10 sec; third and fourth row: they depict results similar to those of the upper two rows, but for negative Dt. Broken horizontal lines correspond to the 99% confidence level.

Fig.1(a)]: (i) Two short-dipoles E_b-W_b, N_b-S_b installed at site 'b' (which lies at a distance of $\approx$ 300m from the site 'c' mentioned in the main text) oriented along EW and NS respectively. (ii) Two dipoles E_b-W_b(-22^o), N_b-S_b(-22^o) installed at the same site 'b', but oriented along directions resulting from a rotation of the EW and NS by 22 degrees anticlockwise and (iii) an electric dipole, labeled E_{bh2}, of length L=50m installed in the borehole bh2 lying $\approx 100m$ SE of site 'c' (cf. similar values were measured in the borehole bh1 lying $\approx$100m NE of site 'c', as mentioned in the main text).

Figure 8 shows the "cr" values calculated by considering the following two time-series: (a) one of the electric dipoles depicted in Fig.3 of the main text and: (b)one of B-field components (oriented along either EW, see Fig. 8(a), or NS, see Fig. 8(b)). An inspection of these results reveals that the same Δt-value is obtained, irrespective of the orientation (as well as the length) of the electric dipole considered. For example, the long dipole $L's - I$ has a length $L \approx$ 5km and is directed almost along NS, while the two long dipoles L, L' -both of which have a length of $\approx$2km, but independent electrodes- are oriented along N30^{o}E.

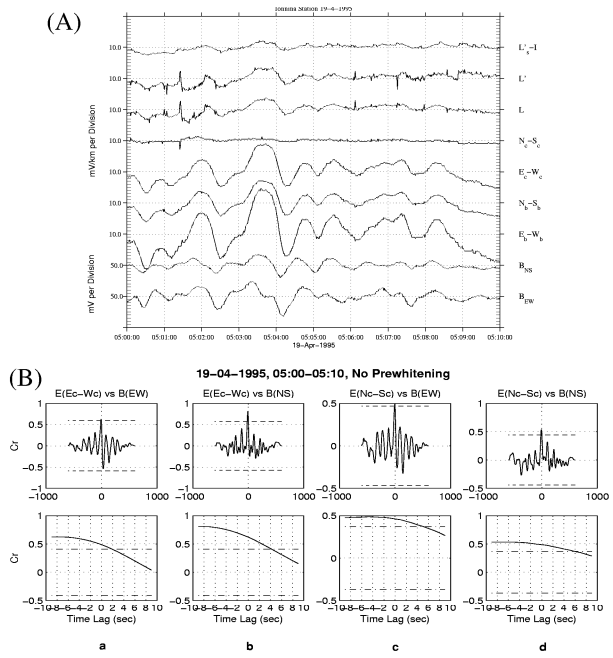

FIG. 7: (A) An example of a 10 min MT disturbance recorded at IOA just before the SES activity of April 19, 1995 (Fig. 1 of the main text) by using two horizontal DMM (i.e., the lower two channels) and the Datalogger 21X acquisition system (with sampling rate 1Hz). (B) Calculated values of "cr" between one horizontal E-field component and one B-field component versus their time-difference Δt (upper: Δt from -1000 to 1000 sec; below: Δt from -10 to 10 sec).

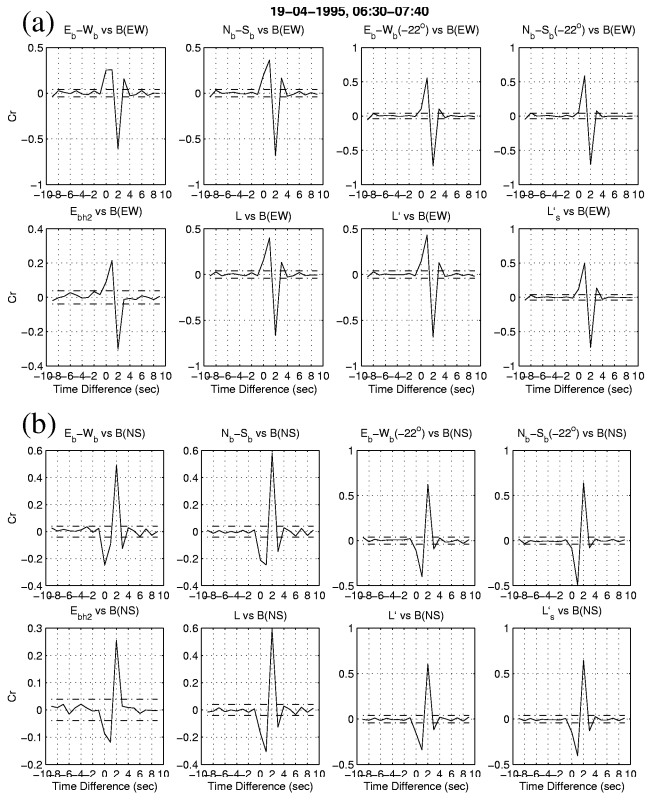

FIG. 8: The calculated "cr" (after prewhitening) between the following two time-series: (i) One E-field component and (ii) one B-filed component (recorded by DMM) versus the time-difference Δt for the SES activity of April 19. The calculation was made by considering the electric dipoles depicted in Fig. 3 of the main text (except of E_c-W_c, N_c-S_c the results of which were presented in Fig. 2 of the main text) and the B-field components oriented along EW (a) or NS (b).

VI. THE CASE OF A CONDUCTIVE CYLINDER EMBEDDED IN A LESS CONDUCTIVE MEDIUM: TIME-DOMAIN

In linear passive media, the electromagnetic fields can be expressed (e.g. see Ref.2) in terms of the source current density $\mathbf{j}(\mathbf{r},t)$ by using the tensor Green's functions $\overleftrightarrow{g}_E(\mathbf{r},\mathbf{r}';t-t')$, $\overleftrightarrow{g}_B(\mathbf{r},\mathbf{r}';t-t')$ for the electric and magnetic field respectively:

$$\mathbf{e}(\mathbf{r},t)=\int_{V'}\int_{-\infty}^{t}\overleftrightarrow{g}_E(\mathbf{r},\mathbf{r}';t-t')\cdot\mathbf{j}(\mathbf{r}',t')d^3\mathbf{r}'dt' \quad (4)$$

$$\mathbf{b}(\mathbf{r},t)=\int_{V'}\int_{-\infty}^{t}\overleftrightarrow{g}_B(\mathbf{r},\mathbf{r}';t-t')\cdot\mathbf{j}(\mathbf{r}',t')d^3\mathbf{r}'dt' \quad (5)$$

A direct application of the convolution theorem yields

$$\mathbf{E}(\mathbf{r},\omega)=\int_{V'}\overleftrightarrow{G}_E(\mathbf{r},\mathbf{r}';\omega)\cdot\mathbf{J}(\mathbf{r}',\omega)d^3\mathbf{r}' \quad (6)$$

$$\mathbf{B}(\mathbf{r},\omega)=\int_{V'}\overleftrightarrow{G}_B(\mathbf{r},\mathbf{r}';\omega)\cdot\mathbf{J}(\mathbf{r}',\omega)d^3\mathbf{r}' \quad (7)$$

for the Fourier transforms $\mathbf{E}$,$\mathbf{B}$,$\mathbf{J}$,$\overleftrightarrow{G}_E$,$\overleftrightarrow{G}_B$ of the time-domain vectors $\mathbf{e}$,$\mathbf{b}$,$\mathbf{j}$, and tensors $\overleftrightarrow{g}_E$,$\overleftrightarrow{g}_B$.

Consider, a circular cylinder of radius R with conductivity σ_p, along the z-axis of a Cartesian system of coordinates with unit vectors $\hat{\mathbf{x}},\hat{\mathbf{y}},\hat{\mathbf{z}}$, embedded in a less conductive medium of conductivity σ. The expressions for $\overleftrightarrow{G}_E$ and $\overleftrightarrow{G}_B$ are, in general, very cumbersome. If we assume, however, that the current source coincides with the cylinder axis, i.e., when $\mathbf{J}(\mathbf{r},\omega)=\delta^2(x,y)I(z,\omega)\hat{\mathbf{z}}$, the forms of $\overleftrightarrow{G}_E\cdot\hat{\mathbf{z}}$, $\overleftrightarrow{G}_B\cdot\hat{\mathbf{z}}$ for $\mathbf{r}'=(\mathbf{r}'\cdot\hat{\mathbf{z}})\hat{\mathbf{z}}$ can be found by a single Bessel function integration. Clearly from Eqs.(4) and (5), the components of the tensor Green's functions $\overleftrightarrow{g}_E(\mathbf{r},\mathbf{r}';t-t')\cdot\hat{\mathbf{z}}$ and $\overleftrightarrow{g}_B(\mathbf{r},\mathbf{r}';t-t')\cdot\hat{\mathbf{z}}$ are equal to the electric and magnetic fields, respectively, that are produced by a point dipole of unit current density $\mathbf{j}(\mathbf{r}',t')=\delta^3(\mathbf{r}')\delta(t')\hat{\mathbf{z}}$. Thus, in the frequency domain, $\overleftrightarrow{G}_E\cdot\hat{\mathbf{z}}$ and $\overleftrightarrow{G}_B\cdot\hat{\mathbf{z}}$ correspond to the solution of the electromagnetic problem (i.e., the electric and magnetic field, respectively) for the current $I(z,\omega)=\delta(z)$. The analytical solution for this case[3] can be expressed in terms of a single component- azimuthally symmetric- vector potential $\mathbf{A}(\rho,\phi,z,\omega)=\hat{\mathbf{z}}A_z(\rho,z,\omega)$, from which the non-zero components of the electromagnetic fields can be

obtained. Assuming that the induction currents are negligible compared to the conduction currents, we have

$$E_z = \rho_l \left(\frac{\partial^2}{\partial^2 z} + \frac{i\mu_0\omega}{\rho_l} \right) A_z \tag{8}$$

$$E_\rho = \rho_l \frac{\partial^2 A_z}{\partial\rho\partial z}, \tag{9}$$

$$B_\phi = -\mu_0 \frac{\partial A_z}{\partial\rho}, \tag{10}$$

where μ_0 is the magnetic permeability of vacuum and ρ_l is equal either to $1/\sigma_p$ or $1/\sigma$ depending on whether Eqs.(9) and (8) are applied for a point inside or outside the cylinder, respectively. The following boundary conditions should be satisfied: 1)the continuity of the tangential electromagnetic field components E_z, B_ϕ, and 2)the current conservation, $j_\rho = E_\rho/\rho_l$ at the surface of the cylinder ($\rho = R$). We then obtain[3] the vector potential inside the cylinder, $\rho \le R$,

$$A_z^{IN}(\rho, z, \ \omega \ ) = \int_0^\infty \frac{i}{R} \cos\left(\lambda\frac{z}{R}\right) H_0^{(1)}\left(n_p\frac{\rho}{R}\right) d\lambda + \int_0^\infty \frac{i}{R} r(\lambda) \cos\left(\lambda\frac{z}{R}\right) J_0\left(n_p\frac{\rho}{R}\right) d\lambda, \tag{11}$$

and outside the cylinder, $\rho > R$,

$$A_z^{OUT}(\rho, z, \omega) = \int_0^\infty \frac{i}{R} T(\lambda) \cos\left(\lambda\frac{z}{R}\right) H_0^{(1)}\left(n\frac{\rho}{R}\right) d\lambda, \tag{12}$$

where $J_n(w)$, $H_n^{(1)}(w)$ are the Bessel and Hankel functions[4] of the first kind of order n, respectively, and $n_p = n_p(\omega,\lambda) = \sqrt{i\mu_0\sigma_p\omega R^2 - \lambda^2}$ and $n = n(\omega,\lambda) = \sqrt{i\mu_0\sigma\omega R^2 - \lambda^2}$. The square root of a complex number w is taken on the 1st Riemann sheet: for $\sqrt{w} = \sqrt{|w|}\exp(i\frac{\arg w}{2})$, $\arg w$ is measured anti-clockwise from the real axis. The functions $r(\lambda)$ and $T(\lambda)$ are

$$r = \frac{\sigma_p n H_0^{(1)}(n) H_1^{(1)}(n_p) - \sigma n_p H_1^{(1)}(n) H_0^{(1)}(n_p)}{\sigma n_p J_0(n_p) H_1^{(1)}(n) - \sigma_p n J_1(n_p) H_0^{(1)}(n)}, \tag{13}$$

$$T = \frac{2in_p\sigma}{\pi\sigma_p n^2 J_1(n_p) H_0^{(1)}(n) - \pi\sigma n n_p J_0(n_p) H_1^{(1)}(n)}. \tag{14}$$

The relations (13) and (14) are just Eqs.(7) and (8) of the main text, if we set $A = r$ and $B = i\pi nT$. The substitution of Eqs.(11) and (12) into Eqs.(8),(9) and (10) yields Eqs.(3), (4) and (5) of the main text.

At this point, we should comment on the physical interpretation of the solution. Since[5]

$$\frac{e^{ik\sqrt{\rho^2+z^2}}}{\sqrt{\rho^2+z^2}} = \int_0^\infty \frac{i}{R} \cos\left(\lambda\frac{z}{R}\right) H_0^{(1)}\left(\sqrt{k^2R^2-\lambda^2}\frac{\rho}{R}\right) d\lambda,$$

the first term of Eq.(11) is just the "singular"- primary- vector potential due to the point dipole located on the axis of the cylinder, whereas its second term represents the secondary field produced by the conductivity discontinuity at $\rho = R$. This discontinuity also shields the fields for $\rho > R$ through $T(\lambda)$ of Eq.(12). This might allow us to interpret the functions $r(\lambda)$ and $T(\lambda)$ as generalized reflection and transmission "coefficients".

Using Eqs.(8)-(10), we obtain the forms of $\overleftrightarrow{G}_E \cdot \hat{\mathbf{z}}(\mathbf{r},\mathbf{r}';\omega)$ and $\overleftrightarrow{G}_B \cdot \hat{\mathbf{z}}(\mathbf{r},\mathbf{r}';\omega)$ presented in Eqs.(3)-(5) of the main text. In general, all these expressions, can employ dispersive relations for σ and σ_p. However, as a first approximation, no frequency dependence was assumed and the values of σ and σ_p were taken (see the main text) comparable to typical values found in the Earth. After calculating- by direct numerical integration of Eqs.(3), (4), (5) of the main text- the non-vanishing components of $\overleftrightarrow{G}_E \cdot \hat{\mathbf{z}}$ and $\overleftrightarrow{G}_B \cdot \hat{\mathbf{z}}$, the relations (6) and (7) have been used to obtain the Fourier transformed electromagnetic field from which, by a numerical inverse-Fourier transform, the time-domain electromagnetic fields shown in Fig. 4 of the main text have been constructed.

For the evaluation of the Bessel functions the module CJYHBS[6] of the National Institute of Standards and Technology Core Math LIBrary (CMLIB) was used, and the numerical integration was adapted to the trigonometric functions involved (cf. the function $Z_\nu(\lambda,\rho;\omega)$ is smooth and in order to obtain an acceptable accuracy the numerical method is focused on the highly oscillating trigonometric functions). The current $i(z,t)$ [i.e., $\mathbf{j}(\mathbf{r},t) = \delta^2(x,y)i(z,t)\hat{\mathbf{z}}$] was a boxcar pulse, $i(z,t) = \delta(z)\Theta(t)\Theta(T_d - t)$, with duration T_d(=11s) comparable to the mean duration of the pulses in SES activities.

The validity of the numerical method employed, was verified by comparing the results obtained, using only the first term of Eq.(11) -primary field-, with those from an analytic expression that holds for a weakly conductive medium of conductivity σ (e.g. see Ref.2). For example, the absolute error in the calculation of $E_z(\rho = 1\text{km}, z = 80\text{km})$, in the arbitrary units presented in Fig.4 of the main text, was always less than 0.0016.

Concerning the plausibility of the model proposed: Aiming at the determination of the geolectric structure beneath the measuring station at IOA, detailed MT-measurements have been carried out.[7] The results obtained, are consistent with the existence of a highly conductive path terminating (below the earth's surface) close to the measuring station.

* Electronic address: pvaro@otenet.gr

[1] EMI, *MT-1, A mobile System for MT Measurements* (Electro Magnetic Instruments, Berkeley, CA, 1995).

[2] P. Varotsos, N. Sarlis, and M. Lazaridou, Phys. Rev. B **59**, 24 (1999).

[3] N. Sarlis, in *Earthquake Thermodynamics and Phase Transformations in the Earth's Interior*, edited by R. Teisseyre and J. Mazewski (Academic Press, San Diego, 2001), p. 463.

[4] M. Abramowitz and I. Stegun, *Handbook of Mathematical Functions* (Dover, New York, 1970).

[5] I. S. Gradshteyn and I. M. Ryzhik, *Table of Integrals, Series, and Products* (Academic Press, San Diego, 1980), pp. 737, Eq.6.677.8.

[6] D. Amos and S. Daniel, FORTRAN subroutine CJYHBS. This program may be retrieved via (http://gams.nist.gov/serve.cgi/Module/CMLIB/CJYHBS/272/).

[7] K. Eftaxias, I. Rokityansky, N. Bogris, G. Balasis, and P. Varotsos, Journal of Atmospheric Electricity **22**, 113 (2002).